


Simulation of Gamma-Ray Transmission Buildup Factors for Stratified Spherical Layers

Dose-Response:
An International Journal
January-March 2022:1–9
© The Author(s) 2022
Article reuse guidelines:
sagepub.com/journals-permissions
DOI: 10.1177/115593258211070911
journals.sagepub.com/home/dos


Abdulrahman A. Alfuraih¹ 

Abstract

Deterministic particle transport codes usually take into account scattered photons with correct attenuation laws and application of buildup factor to incident beam. Transmission buildup factors for adipose, bone, muscle, and skin human tissues, as well as for various combinations of these media for point isotropic photon source with energies of .15, 1.5 and 15 MeV, for different thickness of layers, were carried out using Geant4 (version 10.5) simulation toolkit. Also, we performed the analysis of existing multilayered shield fitting models (Lin and Jiang, Kalos, Burke and Beck) of buildup factor and the proposition of a new model. We found that the model combining those of Burke and Beck, for low atomic number (Z) followed by high Z materials and Kalos 1 for high Z followed by low Z materials, accurately reproduces simulation results with approximated deviation of $3 \pm 3\%$, $2 \pm 2\%$, and $3 \pm 2\%$ for 2, 3, and 4 layers, respectively. Since buildup factors are the key parameter for point kernel calculations, a correct study can be of great interest to the large community of radiation physicists, in general, and to medical imaging and radiotreatment physicists, especially.

Keywords

Geant4, buildup factor, transmission, multilayer, human tissues

Introduction

Nowadays, the most commonly used cancer therapy is the radiotherapy modality, including many forms such as brachytherapy and gamma knife, with almost half of all patients receiving radiation as part of their treatment.^{1,2} From the many existing computational tools used for treatment protocol selection, we cite the Monte Carlo simulation technique³⁻⁸ and point-kernel method.⁹⁻¹¹ The main difference between both techniques concerns the manner of particles transport handling, as 1 of them microscopically resolve the problem, whereas the second has a macroscopic approach. The point-kernel (PK) technique is based on the gamma radiation propagation assumed as beam-like and thus gaining time for decision-taking. From the important parameters forming a PK core, we refer to the buildup factor (BUF) quantifying the scattered to unscattered beam during particle-medium interaction.

Many existing tools have been used for BUF computations, such as PALLAS¹² and ASFIT,¹³ other than Monte Carlo simulation programs (EGS4,¹⁴ Geant4,^{15,16} and MCNPX¹⁷).

Moreover, from the many available modeling of BUF such as the invariant embedding method,^{18,19} the moments method,²⁰ and the iterative method,²¹ we found the more sophisticated one called the geometric progression (GP) fitting method by Harima et al.²²⁻²⁴ Also, as GP fitting methods, we found those provided by Kalos²⁵ and by Burke and Beck²⁶ used for monodirectional parallel-plane beam and stratified shields and the more recent one by Lin and Jiang²⁷ considering the case of isotropic point source and spherical layers. However, the last work does not investigate materials having close densities or atomic number, especially for human tissues and organs (as we can assume

¹Department of Radiological Sciences, College of Applied Medical Science, King Saud University, Riyadh, Saudi Arabia

Corresponding Author:

Abdulrahman A. Alfuraih, Department of Radiological Sciences, College of Applied Medical Science, King Saud University, P.O. Box 10219, Riyadh 11433, Saudi Arabia.
Email: aalfuraih@ksu.edu.sa



Creative Commons Non Commercial CC BY-NC: This article is distributed under the terms of the Creative Commons Attribution-NonCommercial 4.0 License (<https://creativecommons.org/licenses/by-nc/4.0/>) which permits non-commercial use, reproduction and distribution of the work without further permission provided the original work is attributed as specified on the SAGE

and Open Access pages (<https://us.sagepub.com/en-us/nam/open-access-at-sage>).

Table 1. Equivalent Atomic Number (Z_{eq}), 3 GP Fitting Parameters of BUF, Compton, Photoelectric + Pair Production (abs), and Total Attenuation Coefficients (μ_C , μ_{abs} , and μ_T) for 3 Photon Energies and Selected HDRK-Man Tissues.^{29,30}

E (MeV)	Parameter	Adipose	Bone	Muscle	Skin
.15	Z_{eq}	6.486E+0	0 1.153E+1	7.673E+0	7.397E+0
	a	-2.270E-1	-8.400E-2	-1.770E-1	-1.900E-1
	b	4.173E+0	3.104E+0	3.906E+0	3.932E+0
	c	2.657E+0	1.509E+0	2.189E+0	2.294E+0
	d	1.000E-1	1.900E-2	7.300E-2	8.200E-2
	Xk	1.413E+1	1.491E+1	1.436E+1	1.426E+1
	Compton	1.477E-1	1.417E-1	1.460E-1	1.458E-1
	Photo+PP	4.212E-4	3.580E-3	7.872E-4	6.854E-4
	Total	1.481E-1	1.453E-1	1.468E-1	1.465E-1
1.5	Z_{eq}	5.560E+0	8.641E+0	6.586E+0	6.445E+0
	a	7.500E-2	-5.500E-2	-6.200E-2	-6.400E-2
	b	2.038E+0	1.917E+0	1.985E+0	1.991E+0
	c	1.337E+0	1.257E+0	1.286E+0	1.292E+0
	d	3.900E-2	2.200E-2	2.800E-2	2.900E-2
	Xk	1.373E+1	1.463E+1	1.437E+1	1.421E+1
	Compton	5.750E-2	5.533E-2	5.689E-2	5.679E-2
	Photo+PP	8.282E-5	1.265E-4	9.777E-5	9.540E-5
	Total	5.759E-2	5.546E-2	5.699E-2	5.688E-2
15	Z_{eq}	5.507E+0	8.031E+0	6.494E+0	6.369E+0
	a	4.700E-2	5.000E-2	4.700E-2	4.700E-2
	b	1.281E+0	1.265E+0	1.273E+0	1.274E+0
	c	8.360E-1	8.420E-1	8.410E-1	8.410E-1
	d	-2.700E-2	3.900E-2	-3.200E-2	-3.100E-2
	Xk	1.467E+1	1.502E+1	1.515E+1	1.518E+1
	Compton	1.267E-2	1.220E-2	1.254E-2	1.252E-2
	Photo+PP	5.759E-3	7.792E-3	6.606E-3	6.478E-3
	Total	1.843E-2	1.999E-2	1.915E-2	1.900E-2

water medium for approximating the majority of them). Other fitting methods, which do not take into account the orientation of consecutive layers in terms of atomic number,²⁸ were not included in this work. It is the aim of this paper to propose a new empirical formula to reproduce buildup factors of stratified spherical shields for a point isotropic source so that it can be built into the presently widely applied point-kernel codes to resolve their deficiency in handling the buildup effect for stratified shields. Simple and easy application are the major concerns of the new empirical formula. Buildup factors of stratified shields are synthesized from those of the existing single-layered shields in a conventional form.

The main goal of this work was to propose a new modified model able to reproduce directly Geant4-based simulations of BUF for multilayered gamma-ray attenuators. Thus, we focused on the following 3 items: (i) Geant4 simulations; (ii) comparison against Lin and Jiang; Kalos and Burke and Beck models; and (iii) proposition of a modified fitting model. For that, 4 typically selected human tissues representing high, medium, and low atomic number (adipose, bone, muscle, and skin), were simulated for different configurations of isotropic point source with energies .15, 1.5, and 15MeV and 2, 3, and 4 layers as concentric spheres around the gamma-ray source. Moreover, an optimization procedure of the GP fitting parameters to calculate multilayer BUF from individual material

BUF was proposed at the end of this work. However, our study was limited to small thickness (up to 8 mfp); the current work can be considered as a continuation on the attention made by radiation physicists, especially in terms of point kernel-based treatment planning and diagnosis imaging purposes.

Materials and Methods

Used human tissues of adipose, bone, muscle, and skin have an equivalent atomic number given in Table 1 and an elemental composition taken from the literature.²⁹

Three isotropic point source energies were considered: .15, 1.5, and 15 MeV. Also, the same procedure for Z_{eq} calculation, described in our previous work,¹⁶ has been followed.

Briefly, such procedure was based on *Log-Log* interpolation in terms of elemental atomic number and Compton to total attenuation coefficient ratio search (μ_C/μ_T), for a given photon energy. Here, we will describe the Geant4-based simulation procedure carried out and enumerate the proposed parameterization (fitting) models of BUF for n concentric spherical layers including an isotropic point source at the center.

Simulation Procedure

Geant4 version 10.5 was used to mimic the transport of gamma rays isotropically from a point source through a given simple or

Table 2. Comparison of BUF Simulated Using Geant4 Against Other Model Data for Double Layered Shields and 3 Photon Energies. LJ: Lin and Jiang,²⁷ K: Kalos,²⁵ BB: Burke and Beck,²⁶ M_1 - M_6 : 6 Proposed Models (A: Adipose, B: Bone, M: Muscle, S: Skin, IM+2B Means 1 mfp M Followed by 2 mfp B).

E (MeV)	Med+Med2	G4	LJ	K	BB	M1	M2	M3	M4	M5	M6
.15	IM+1B	3.38	3.85	3.74	4.08	3.85	3.85	3.74	3.74	4.08	4.08
	IM+2B	5.99	5.86	6.11	6.35	5.86	5.86	6.11	6.11	6.35	6.35
	IM+3B	8.70	8.41	9.14	9.26	8.41	8.41	9.14	9.14	9.26	9.26
	2M+2B	9.07	8.61	8.82	9.43	8.61	8.61	8.82	8.82	9.43	9.43
	2M+3B	12.38	11.53	12.71	13.03	11.53	11.53	12.71	12.71	13.03	13.03
	1B+1M	4.17	4.63	4.45	5.08	4.45	5.08	4.63	5.08	4.63	4.45
	1B+2M	7.40	8.45	7.74	9.03	7.74	9.03	8.45	9.03	8.45	7.74
	1B+3M	12.04	14.05	12.39	14.40	12.39	14.40	14.05	14.40	14.05	12.39
	2B+2M	11.30	12.89	11.33	14.14	11.33	14.14	12.89	14.14	12.89	11.33
	2B+2M	17.55	20.83	17.28	21.60	17.28	21.60	20.83	21.60	20.83	17.28
	1M+1A	4.40	5.02	4.86	5.62	4.86	5.62	5.02	5.62	5.02	4.86
	1M+2A	7.98	9.18	8.68	10.29	8.68	10.29	9.18	10.29	9.18	8.68
	1M+3A	13.33	15.38	14.29	16.91	14.29	16.91	15.38	16.91	15.38	14.29
	2M+2A	13.12	15.11	13.91	17.76	13.91	17.76	15.11	17.76	15.11	13.91
	2M+3A	20.70	24.27	21.73	27.86	21.73	27.86	24.27	27.86	24.27	21.73
	1A+1S	4.30	4.48	4.33	4.76	4.48	4.48	4.33	4.33	4.76	4.76
	1A+2S	7.47	7.63	7.91	8.26	7.63	7.63	7.91	7.91	8.26	8.26
	1A+3S	11.98	12.14	13.02	13.23	12.14	12.14	13.02	13.02	13.23	13.23
	2A+2S	12.11	11.86	12.39	13.27	11.86	11.86	12.39	12.39	13.27	13.27
	2A+3S	18.19	17.72	19.58	20.10	17.72	17.72	19.58	19.58	20.10	20.10
1.5	IM+1B	2.58	2.54	2.48	2.64	2.54	2.54	2.48	2.48	2.64	2.64
	IM+2B	3.50	3.45	3.51	3.60	3.45	3.45	3.51	3.51	3.60	3.60
	IM+3B	4.50	4.45	4.61	4.65	4.45	4.45	4.61	4.61	4.65	4.65
	2M+2B	4.49	4.33	4.45	4.65	4.33	4.33	4.45	4.45	4.65	4.65
	2M+3B	5.55	5.37	5.67	5.76	5.37	5.37	5.67	5.67	5.76	5.76
	1B+1M	2.65	2.73	2.67	2.95	2.67	2.95	2.73	2.95	2.73	2.67
	1B+2M	3.65	3.81	3.69	4.11	3.69	4.11	3.81	4.11	3.81	3.69
	1B+3M	4.72	4.95	4.78	5.28	4.78	5.28	4.95	5.28	4.95	4.78
	2B+2M	4.72	4.99	4.74	5.60	4.74	5.60	4.99	5.60	4.99	4.74
	2B+3M	5.88	6.25	5.89	6.92	5.89	6.92	6.25	6.92	6.25	5.89
	1M+1A	2.65	2.76	2.70	2.99	2.70	2.99	2.76	2.99	2.76	2.70
	1M+2A	3.65	3.84	3.73	4.18	3.73	4.18	3.84	4.18	3.84	3.73
	1M+3A	4.72	5.00	4.85	5.37	4.85	5.37	5.00	5.37	5.00	4.85
	2M+2A	4.73	5.06	4.83	5.75	4.83	5.75	5.06	5.75	5.06	4.83
	2M+3A	5.88	6.31	6.01	7.09	6.01	7.09	6.31	7.09	6.31	6.01
	1A+1S	2.61	2.58	2.52	2.69	2.58	2.58	2.52	2.52	2.69	2.69
	1A+2S	3.58	3.54	3.61	3.71	3.54	3.54	3.61	3.61	3.71	3.71
	1A+3S	4.62	4.60	4.76	4.81	4.60	4.60	4.76	4.76	4.81	4.81
	2A+2S	4.61	4.45	4.59	4.80	4.45	4.45	4.59	4.59	4.80	4.80
	2A+3S	5.72	5.55	5.87	5.97	5.55	5.55	5.87	5.87	5.97	5.97
15	IM+1B	1.58	1.57	1.56	1.61	1.57	1.57	1.56	1.56	1.61	1.61
	IM+2B	1.82	1.80	1.83	1.85	1.80	1.80	1.83	1.83	1.85	1.85
	IM+3B	2.05	2.03	2.08	2.09	2.03	2.03	2.08	2.08	2.09	2.09
	2M+2B	2.05	1.99	2.06	2.10	1.99	1.99	2.06	2.06	2.10	2.10
	2M+3B	2.28	2.22	2.32	2.34	2.22	2.22	2.32	2.32	2.34	2.34
	1B+1M	1.59	1.60	1.59	1.67	1.59	1.67	1.60	1.67	1.60	1.59
	1B+2M	1.84	1.85	1.83	1.93	1.83	1.93	1.85	1.93	1.85	1.83
	1B+3M	2.09	2.08	2.06	2.17	2.06	2.17	2.08	2.17	2.08	2.06
	2B+2M	2.09	2.10	2.07	2.27	2.07	2.27	2.10	2.27	2.10	2.07
	2B+3M	2.33	2.33	2.30	2.52	2.30	2.52	2.33	2.52	2.33	2.30
	1M+1A	1.57	1.60	1.59	1.67	1.59	1.67	1.60	1.67	1.60	1.59
	1M+2A	1.81	1.84	1.83	1.93	1.83	1.93	1.84	1.93	1.84	1.83
	1M+3A	2.04	2.07	2.05	2.16	2.05	2.16	2.07	2.16	2.07	2.05
	2M+2A	2.04	2.08	2.06	2.26	2.06	2.26	2.08	2.26	2.08	2.06
	2M+3A	2.27	2.31	2.28	2.50	2.28	2.50	2.31	2.50	2.31	2.28
	1A+1S	1.58	1.56	1.55	1.60	1.56	1.56	1.55	1.55	1.60	1.60
	1A+2S	1.83	1.79	1.82	1.84	1.79	1.79	1.82	1.82	1.84	1.84
	1A+3S	2.06	2.02	2.06	2.07	2.02	2.02	2.06	2.06	2.07	2.07
	2A+2S	2.07	1.98	2.03	2.08	1.98	1.98	2.03	2.03	2.08	2.08
	2A+3S	2.30	2.20	2.29	2.31	2.20	2.20	2.29	2.29	2.31	2.31

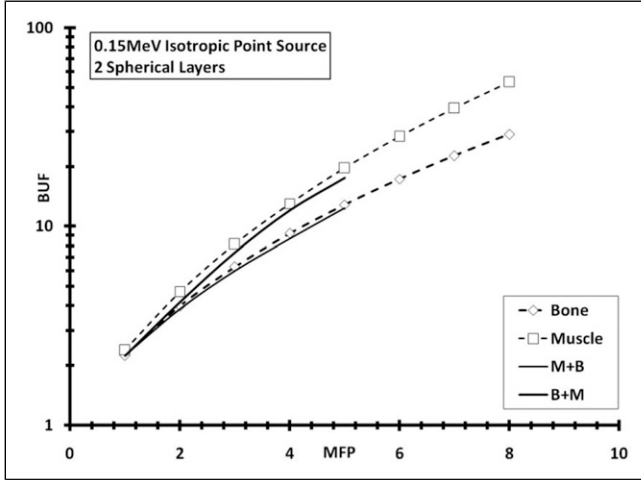


Figure 1. Geant4 simulated BUF for 2 spherical layers' function of thickness (in mfp) for .15 MeV isotropic point source energy. Monolayer BUF was also plotted for bone (B) and muscle (M).

group of media. The geometry of the problem, for monolayer cases, consists of a monoenergetic point source located at the center of ten concentric spheres, separated by 1 mfp for each step. For multilayer arrangements, we superposed consecutively spherical layers with specific thickness for each medium. We tracked the full history of gamma rays through the setup in order to compute the photon flux crossing each shell/surface of the medium. Then, each crossed photon energy has been internally (within *SteppingAction* class) converted into exposure. However, the BUF calculation needs the knowledge of transmission flux in the presence and in absence of the medium; we repeated computations for the air medium in place of each medium keeping the same setup characteristics (geometrical thickness). In this study, the buildup factor was computed for 10^9 gamma rays per run. We activated all the physical processes for electrons and photons. We used the *G4EmStandardPhysics_option3* built-in physics library with a cutoff of 1 keV for electrons and photons. The overall statistical uncertainty does not exceed 1% in any case.

Proposed Parameterization Models

The general BUF formula for multilayers can be written in the following form:

$$B\left(\sum_{i=1}^{n-1} X_i, X_n\right) = B_n(X_n) + \left[B_n\left(\sum_{i=1}^n X_i\right) - B_n(X_n)\right] \times K \times C_n, \quad (1)$$

with the geometric progression parameter

$$K = \frac{B\left(\sum_{i=1}^{n-2} X_i, X_{n-1}\right) - 1}{B_n\left(\sum_{i=1}^{n-1} X_i\right) - 1}, \quad (2)$$

where X_1, X_2, \dots, X_n are the thickness of n consecutive material forming the multilayered shield. The correction parameter, C_n , has mainly 3 existing models, and its global form depends on Z_{eq} of consecutive layers (HZ/LZ means the arrangement of medium with high Z_{eq} followed by medium with low Z_{eq}). Three different existing (Lin and Jiang, Kalos, and Burke and Beck) and 6 proposed (M_1 - M_6) fitting models were used for comparison and optimization purposes (against directly Geant4-simulated results), and their formula can be written as follows:

1. Kalos²⁵:

$$C_n = \begin{cases} 1.0, & \text{HZ/LZ} \\ e^{-1.7X_n} + (\gamma\beta/K)(1 - e^{-X_n}), & \text{LZ/HZ} \end{cases} \quad (3)$$

2. Burke and Beck²⁶:

$$C_n = \begin{cases} e^{-\frac{X_n}{7}} + 1.5(1 - e^{-X_n}), & \text{HZ/LZ} \\ e^{-\gamma X_n} + (\gamma\beta/K)(1 - e^{-X_n}), & \text{LZ/HZ} \end{cases} \quad (4)$$

3. Lin and Jiang²⁷:

$$C_n = \begin{cases} e^{(-1.08\beta X_n)} + 1.13\beta\ell(X_n), & \text{HZ/LZ} \\ (\gamma/K)e^{-X_n} + 0.8\ell(X_n), & \text{LZ/HZ} \end{cases} \quad (5)$$

4. M_1 :

$$C_n = \begin{cases} 1.0, & \text{HZ/LZ} \\ (\gamma/K)e^{-X_n} + 0.8\ell(X_n), & \text{LZ/HZ} \end{cases} \quad (6)$$

5. M_2 :

$$C_n = \begin{cases} e^{-\frac{X_n}{7}} + 1.5(1 - e^{-X_n}), & \text{HZ/LZ} \\ (\gamma/K)e^{-X_n} + 0.8\ell(X_n), & \text{LZ/HZ} \end{cases} \quad (7)$$

6. M_3 :

$$C_n = \begin{cases} e^{(-1.08\beta X_n)} + 1.13\beta\ell(X_n), & \text{HZ/LZ} \\ e^{-1.7X_n} + (\gamma\beta/K)(1 - e^{-X_n}), & \text{LZ/HZ} \end{cases} \quad (8)$$

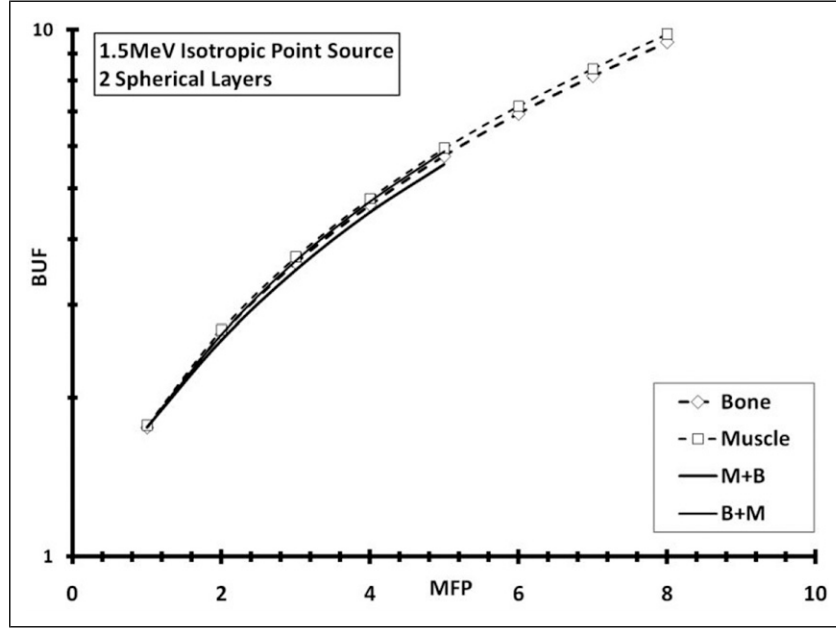


Figure 2. Geant4 simulated BUF for 2 spherical layers' function of thickness (in mfp) for 1.5 MeV isotropic point source energy. Monolayer BUF was also plotted for bone (B) and muscle (M).

7. M_4 :

$$C_n = \begin{cases} e^{-X_n^2} + 1.5(1 - e^{-X_n}), HZ/LZ \\ e^{-1.7X_n} + (\gamma\beta/K)(1 - e^{-X_n}), LZ/HZ \end{cases} \quad (9)$$

8. M_5 :

$$C_n = \begin{cases} e^{(-1.08\beta X_n)} + 1.13\beta\ell(X_n), HZ/LZ \\ e^{-\gamma X_n} + (\gamma\beta/K)(1 - e^{-X_n}), LZ/HZ \end{cases} \quad (10)$$

9. M_6 :

$$C_n = \begin{cases} 1.0, HZ/LZ \\ e^{-\gamma X_n} + (\gamma\beta/K)(1 - e^{-X_n}), LZ/HZ \end{cases} \quad (11)$$

with

$$\gamma = \frac{(\mu_C/\rho)_{n-1}}{(\mu_C/\rho)_n}, \quad (12)$$

$$\beta = \frac{(\mu_t/\rho)_{n-1}}{(\mu_C/\rho)_n}, \quad (13)$$

and

$$\ell(X_n) = \frac{B_n(X_n)+1}{B_{n-1}(X_n)+1} (1 - e^{-X_n}), \quad (14)$$

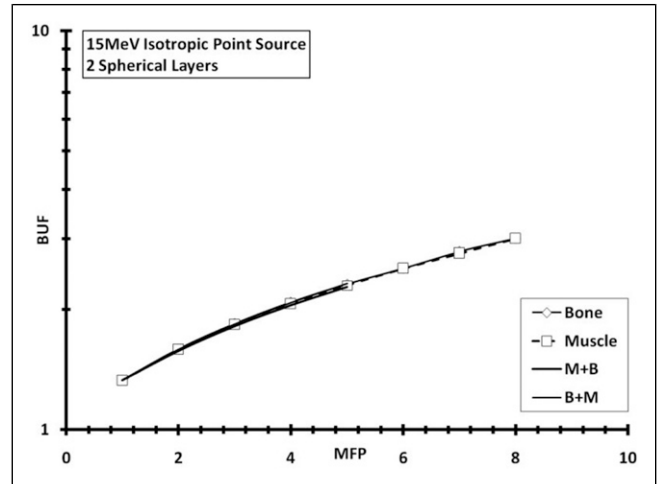


Figure 3. Geant4 simulated BUF for 2 spherical layers' function of thickness (in mfp) for 15 MeV isotropic point source energy. Monolayer BUF was also plotted for bone (B) and muscle (M).

with μ_C/ρ and μ_t/ρ as the Compton and the total mass attenuation coefficient, respectively.

Results and Discussion

Monolayers and Bilayers Simulation

Geometric progression fitting parameters of BUF for adipose, bone, muscle, and skin HDRK-Man tissues^{29,30} were extracted from the previous work,¹⁶ and results are provided in Table 1. Then, BUF for bilayers was fully simulated (using Geant4) and

Table 3. Comparison of BUF Simulated Using Geant4 Against Other Model Data for 3 Layered Shields and 3 Photon Energies. LJ: Lin and Jiang,²⁷ K: Kalos,²⁵ BB: Burke and Beck,²⁶ M_1 - M_6 : 6 proposed models (A: Adipose, B: Bone, M: Muscle, S: Skin, IB+IM+2A means 1 mfp B followed by 1 mfp M followed by 2 mfp A).

E (MeV)	Med1+Med2+Med3+Med4	G4	LJ	K	BB	MI	M2	M3	M4	M5	M6
.15	IB+IM+IA+IS	7.68	8.68	8.01	11.08	8.01	11.08	8.68	11.08	8.68	8.01
	IB+IM+2A	13.12	14.92	13.29	19.05	13.29	19.05	14.92	19.05	14.92	13.29
	IB+IM+3A	20.91	23.98	20.84	29.78	20.84	29.78	23.98	29.78	23.98	20.84
	IB+2M+3A	31.03	37.34	30.36	46.66	30.36	46.66	37.34	46.66	37.34	30.36
	IA+IM+IB	6.36	6.01	5.68	6.66	6.01	6.01	5.68	5.68	6.66	6.66
	IA+IM+2B	8.94	8.33	8.80	9.43	8.33	8.33	8.80	8.80	9.43	9.43
	IA+IM+3B	12.16	11.18	12.71	13.03	11.18	11.18	12.71	12.71	13.03	13.03
	IA+2M+3B	16.78	15.08	17.12	17.71	15.08	15.08	17.12	17.12	17.71	17.71
1.5	IB+IM+1A	3.69	3.89	3.70	4.71	3.70	4.71	3.89	4.71	3.89	3.70
	IB+IM+2A	4.79	5.12	4.81	6.21	4.81	6.21	5.12	6.21	5.12	4.81
	IB+IM+3A	5.95	6.38	5.99	7.60	5.99	7.60	6.38	7.60	6.38	5.99
	IB+2M+3A	7.17	7.84	7.20	9.64	7.20	9.64	7.84	9.64	7.84	7.20
	IA+IM+IB	3.49	3.35	3.24	3.61	3.35	3.35	3.24	3.24	3.61	3.61
	IA+IM+2B	4.47	4.24	4.44	4.65	4.24	4.24	4.44	4.44	4.65	4.65
	IA+IM+3B	5.52	5.27	5.76	5.76	5.27	5.27	5.67	5.67	5.76	5.76
	IA+2M+3B	6.64	6.19	6.80	6.94	6.19	6.19	6.80	6.80	6.94	6.94
15	IB+IM+1A	1.81	1.86	1.83	2.07	1.83	2.07	1.86	2.07	1.86	1.83
	IB+IM+2A	2.03	2.09	2.06	2.35	2.06	2.35	2.09	2.35	2.09	2.06
	IB+IM+3A	2.26	2.32	2.28	2.59	2.28	2.59	2.32	2.59	2.32	2.28
	IB+2M+3A	2.47	2.58	2.52	2.97	2.52	2.97	2.58	2.97	2.58	2.52
	IA+IM+IB	1.84	1.77	1.76	1.86	1.77	1.77	1.76	1.76	1.86	1.86
	IA+IM+2B	2.09	1.97	2.05	2.10	1.97	1.97	2.05	2.05	2.10	2.10
	IA+IM+3B	2.34	2.20	2.32	2.34	2.20	2.20	2.32	2.32	2.34	2.34
	IA+2M+3B	2.58	2.38	2.59	2.59	2.38	2.38	2.56	2.56	2.59	2.59

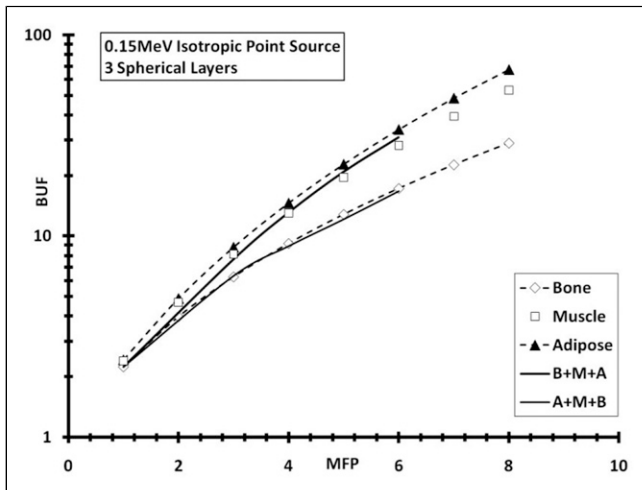


Figure 4. Geant4 simulated BUF for 3 spherical layers' function of thickness (in mfp) for .15 MeV isotropic point source energy. Monolayer BUF was also plotted for adipose (A), bone (B), and muscle (M).

fitted according to different cited models, for .15, 1.5, and 15 MeV point isotropic photon source energy and different thickness combinations. Results are tabulated in Table 2, and Figures 1-3 show also BUF for monolayers of bone and muscle tissues.

We confirmed previous explanation presented by Mann,^{28,31} illustrating that BUF for muscle was higher than

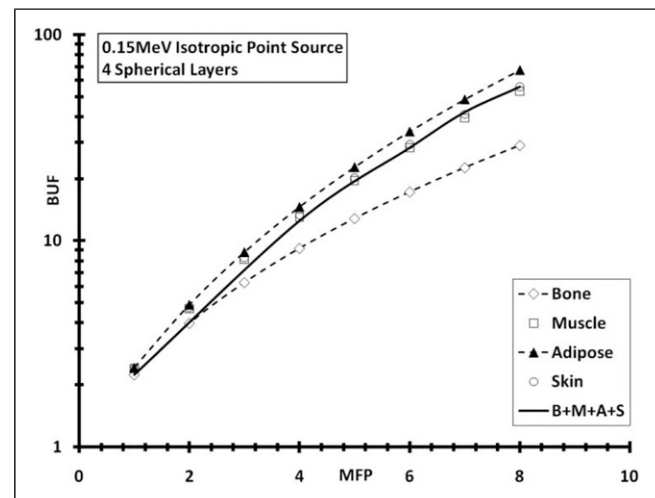


Figure 5. Geant4 simulated BUF for 4 spherical layers' function of thickness (in mfp) for .15 MeV isotropic point source energy. Monolayer BUF was also plotted for adipose (A), bone (B), muscle (M), and skin (S).

that for bone tissue, due to the higher value of *Compton* mass attenuation coefficient μ_C and the lower value of *Photoelectric* and *Pair Production* mass attenuation coefficient μ_{PP} of muscle, as given in Table 1. This is due to the fact that *Compton* effect increases the scattering phenomena

Table 4. Comparison of BUF Simulated Using Geant4 Against Other Model Data for 4 Layered Shields and 3 Photon Energies: LJ: Lin and Jiang,²⁷ K: Kalos,²⁵ BB: Burke and Beck,²⁶ M_1 - M_6 : 6 Proposed Models (A: Adipose, B: Bone, M: Muscle, S: Skin, IB+IM+2A+2S Means 1 mfp B Followed by 1 mfp M Followed by 2 mfp A Followed by 2 mfp S).

E (MeV)	Med1+Med2+Med3+Med4	G4	LJ	K	BB	M1	M2	M3	M4	M5	M6
.15	IB+IM+IA+IS	12.51	12.18	11.18	14.72	11.68	13.97	11.36	12.01	13.42	13.06
	IB+IM+2A+2S	28.28	26.84	26.83	30.78	24.65	32.40	26.94	27.22	26.69	29.26
	IB+IM+3A+3S	54.34	53.06	55.16	58.38	47.28	63.75	55.21	55.30	57.67	57.28
	IB+2M+3A+IS	42.07	42.06	34.53	50.00	37.23	48.50	36.29	38.63	45.33	41.84
	IB+2M+3A+2S	55.81	57.14	52.01	61.35	48.50	68.73	52.44	53.02	59.07	57.37
1.5	IB+IM+IA+IS	4.73	4.54	4.24	5.20	4.43	5.00	4.28	4.45	4.87	4.79
	IB+IM+2A+2S	7.04	6.65	6.73	7.39	6.41	7.54	6.74	6.78	7.22	7.17
	IB+IM+3A+3S	9.58	8.93	9.47	9.81	8.58	10.05	9.47	9.48	9.74	9.72
	IB+2M+3A+IS	8.35	7.98	7.21	9.37	7.63	8.96	7.34	7.69	8.67	8.42
	IB+2M+3A+2S	9.62	9.01	9.01	10.07	8.51	10.43	9.04	9.10	9.80	9.71
15	IB+IM+IA+IS	2.05	1.99	1.95	1.95	2.16	1.97	2.08	1.99	2.09	2.08
	IB+IM+2A+2S	2.51	2.39	2.47	2.47	2.60	2.37	2.55	2.48	2.57	2.56
	IB+IM+3A+3S	2.96	2.83	3.04	3.04	3.10	2.80	3.02	3.04	3.09	3.09
	IB+2M+3A+IS	2.72	2.63	2.55	2.55	2.96	2.60	2.81	2.56	2.83	2.81
	IB+2M+3A+2S	2.95	2.82	2.95	2.95	3.15	2.78	3.08	2.95	3.10	3.09

Table 5. Global Statistical Analysis (Average and Standard Deviation) of Different Models for 2, 3, and 4 Layers in Spherical Geometry and Isotropic Point Source.

			2 Layers	3 Layers	4 Layers
	Lin and Jiang	Average	6	8	19
		StdDev	5	9	20
	Kalos	Average	6	8	18
		StdDev	5	7	19
	Burke and Beck	Average	6	10	22
		StdDev	6	11	22
This work	LH(L)/HL(K)	Average	6	8	17
		StdDev	5	7	17
	LH(L)/HL(K)	Average	6	10	23
		StdDev	5	11	24
	LH(L)/HL(K)	Average	6	9	19
		StdDev	5	9	19
	LH(L)/HL(K)	Average	6	10	19
		StdDev	6	11	20
	LH(L)/HL(K)	Average	6	9	21
		StdDev	5	9	21
	LH(L)/HL(K)	Average	6	8	20
		StdDev	5	7	21

(described by BUF), whereas the absorption effect (*Photoelectric + Pair Production*) decreases it, which is clearly visible when going through the above cited figures. Moreover, combining muscle followed by bone tissues, in Figure 1, leads to lower BUF than for the reverse order of combination. This can be explained by the fact that a large number of scattered photons were produced within the first medium; however, they will be eliminated and absorbed by the second medium. On the other hand, we can see that BUF decreased, for a given thickness, when energy increased, as the ratio of Z_{eq} (bone to muscle), as given in Table 1, decreased from 1.503 to 1.312 to 1.237, producing more and

more closer BUF values. Also, BUF for 2 layers was found between both limits corresponding to BUF for single layers. Moreover, we clearly see a trend similarity of BUF for muscle followed by bone and adipose followed by skin, especially for deep locations where BUF values become larger.

Trilayer Simulation

Table 3 illustrates BUF simulated, using Geant4, and computed using 9 fitting models for different combinations of bone, muscle, and adipose, at energies of .15, 1.5, and 15 MeV.

From that table and Figure 4, we can reconfirm the location of global BUF (corresponding to different combinations) between those for bone and adipose, having highest and lowest Z_{eq} , respectively. We can also notice that global BUF at higher photon energy becomes closer to those for individual layers, Z_{eq} , as scattering and absorption processes become similar.

On the other hand, for .15 MeV photon energy, the arrangement of bone ($Z_{eq} = 11.530$) followed by muscle ($Z_{eq} = 7.673$) followed by adipose ($Z_{eq} = 6.486$), we observed higher BUF values and rapid growth for deep penetrations than for the inverse order of arrangement, allowing us to reconfirm the hypothesis of applying the BUF function of bilayers to that of trilayers. Also, from Tables 2 and 3, for example, we can consider B+M+A arrangement as 2 layers with HZ followed by LZ, that is, B+M followed by A or B followed by M+A.

Multilayer Simulation

Also, Figure 5 and Table 4 show the middle location of global BUF between those for adipose and bone tissues. Moreover, previous interpretation (trilayer case) can be applied for actual situation. In order to optimize a best fitting model to reproduce data simulated with Geant4, the statistical analysis, in terms of average and standard deviation, of different models for 2, 3, and 4 layers in spherical geometry and isotropic point source, has been reported in Table 5.

We can see that M_6 model has the best statistical analysis parameters, compared to those for Kalos model, which fails for the number of layers more than 3, and the worst one, for our situations of energy and thickness ranges, was for the Burke and Beck model. The main limitation of this work concerns the study of short penetration depths, so a straightforward extension to higher thickness could be conducted to be more consistent and justify our conclusions.

Conclusion

Buildup factor of a material for gamma-ray attenuation is an important parameter to describe scattered beam. During this work, the evaluation of gamma-ray buildup factors of stratified human tissue layers for a point isotropic source has been carried out using Geant4. Moreover, we proposed a fitting method able to accurately reproduce Geant4-based simulation results better than existing ones of Li and Jiang, Kalos, and Burcke and Beck models. The proposed fitting model M_6 , leading to an average deviation (according to direct simulation outputs) not exceeding $3 \pm 3\%$ for all studied cases, can be considered the better one of the 9 models. However, the reproducibility procedure should be extended to thickness and photon energies higher than 8 mfp and 15 MeV, adopted here, respectively. Nevertheless, we can consider that proposed results are important for medical imaging and radiation treatment planning for the most existing examination scenario.

Declaration of Conflicting Interests

The author declared no potential conflicts of interest with respect to the research, authorship, and/or publication of this article.

Funding

The author disclosed receipt of the following financial support for the research, authorship, and/or publication of this article. This work was supported by the College of Applied Medical Sciences Research Center and the Deanship of Scientific Research at King Saud University, Saudi Arabia.

ORCID iD

Abdulrahman A. Alfuraih  <https://orcid.org/0000-0003-3010-0136>

References

- Lewin TD, Byrne HM, Maini PK, Caudell JJ, Moros EG, Enderling H. The importance of dead material within a tumour on the dynamics in response to radiotherapy. *Phys Med Biol.* 2020;65(1):015007.
- Fowler JF. Development of radiobiology for oncology—a personal view. *Phys Med Biol.* 2006;51(13):R263-R286.
- Liang Y, Muhammad W, Hart GR, et al. A general-purpose Monte Carlo particle transport code based on inverse transform sampling for radiotherapy dose calculation. *Sci Rep.* 2020;10:9808.
- Hanin LG. A stochastic model of tumor response to fractionated radiation: limit theorems and rate of convergence. *Math Biosci.* 2004;191:1-17.
- O'Rourke SFC, McAnaney H, Hillen T. Linear quadratic and tumour control probability modelling in external beam radiotherapy. *J Math Biol.* 2009;58:799-817.
- Zaider M, Hanin L. Tumor control probability in radiation treatment. *Med Phys.* 2011;38:574-583.
- Gong J, Dos Santos MM, Finlay C, Hillen T. Are more complicated tumour control probability models better? *Math Med Biol.* 2013;30:1-19.
- Bobadilla AVP, Maini PK, Byrne H. A stochastic model for tumour control probability that accounts for repair from sub-lethal damage. *Math Med Biol.* 2018;35:181-202.
- Debus C, Oelfke U, Bartzsch S. A point kernel algorithm for microbeam radiation therapy. *Phys Med Biol.* 2017;62:8341-8359.
- Gotz TI, Schmidkonz C, Chen S, Al-Baddai S, Kuwert T, Lang EW. A deep learning approach to radiation dose estimation. *Phys Med Biol.* 2020;65(3):035007.
- Akhavanallaf A, Shiri I, Arabi H, Zaidi H. Whole-body voxel-based internal dosimetry using deep learning. *Eur J Nucl Med Mol Imag.* 2020;48(3):670-682.
- Takeuchi K, Tanaka S. PALLAS-ID(VII), a code for direct integration of transport equation in one dimensional plane and spherical geometries. *JAERI-*. 1984;M84:214.
- Gopinath DV, Samthanam K. Radiation transport in one dimensional finite technique. *Nucl Sci Eng.* 1971;43(2):186.

14. Nelson WR, Hirayama H, Rogers D. *The EGS4 Code System, SLAC-265*. Menlo Park, CA: Stanford Linear Accelerator Center; 1985.
15. Agostinelli S, Allison J, Amako K, et al. Geant4-a simulation toolkit. *NIMA*. 2003;506(3):250-303.
16. Kadri O, Alfuraih A. Photon energy absorption and exposure buildup factors for deep penetration in human tissues. *Nucl Sci Tech*. 2019;30:176.
17. Moradi F, Khandaker MU, Alrefae T, Ramazanian H, Bradley DA. Monte Carlo simulations and analysis of transmitted gamma ray spectra through various tissue phantoms. *Appl Radiat Isot*. 2019;146:120-126.
18. Sakamoto Y, Tanaka S, Harima Y. Interpolation of gamma ray buildup factors for isotropic source with respect to atomic number. *Nucl Sci Eng*. 1988;100(1):33-42.
19. Shimizu A. Calculations of gamma-ray buildup factors up to depths of 100 mfp by the method of invariant embedding, (I) analysis of accuracy and comparison with other data. *J Nucl Sci Technol*. 2002;39:477-486.
20. Eisenhauer CM, Simmons GL. Point isotropic gamma ray buildup factors in concrete. *Nucl Sci Eng*. 1975;56(3):263-270.
21. Suteau C, Chiron M. An iterative method for calculating gamma ray buildup factors in multi-layer shields. *Radiat Protect Dosim*. 2005;116(1-4):489-492.
22. Harima Y, Sakamoto Y, Tanaka S, et al. Validity of the geometric progression formula in approximating gamma ray buildup factors. *Nucl Sci Eng*. 1986;94:24-35.
23. Harima Y. A historical review and current status of build-up factor calculations and applications. *Radiat Phys Chem*. 1993;41:631-672.
24. Saleh HH, Sharaf JM, Abady RS. Gamma-ray buildup factor and radiation absorbed dose enhancement at tissue-bone interfaces. *Appl Radiat Isot*. 2021;167:109464.
25. Kalos MH. A Monte Carlo calculation of the transport of gamma rays. *NDA* 1957;56-10.
26. Burke GP, Beck HL. Calculated and measured dose buildup factors for gamma rays penetrating multilayered slabs. *Nucl Sci Eng*. 1974;53:109-112.
27. Uei-Tyng Lin L, Shiang-Huei J. A dedicated empirical formula for -ray buildup factors for a point isotropic source in stratified shields. *Radiat Phys Chem*. 1996;48(4):389-401.
28. Mann KS, Mann SS, Py-MLBUF. Development of an online-platform for gamma-ray shielding calculations and investigations. *Ann Nucl Energy*. 2021;150:107845.
29. Hammerstein GR, Miller DW, White DR, Masterson ME, Woodard DR, Laughlin DR. Absorbed radiation dose in mammography. *Radiology*. 1979;130(2):485-491.
30. Kim CH, Choi SH, Jeong JH, Lee C, Chung MS. HDRK-man: a whole body voxel model based on high-resolution color slice images of a Korean adult male cadaver. *Phys Med Biol*. 2008; 53(15):4093-4106.
31. Mann K, Heer M, Rani A. Gamma-ray double-layered transmission exposure buildup factors of some engineering materials, a comparative study. *Radiat Phys Chem*. 2016;125: 27-40.